REDIN Revista Facultad de Ingeniería Universidad de Antioquia

No.116, pp. 100-109, Jul-Sep 2025

Numerical analysis of ice accretion on an airfoil: A case study

Análisis numérico de formación de hielo sobre un perfil aerodinámico: un caso de estudio

Lucas Farabello[1], **Ana Scarabino**[1*], **Federico Bacchi**[2]

[1]Grupo de Fluidodinámica Computacional GFC, Facultad de Ingeniería, Universidad Nacional de La Plata. Calle 116 entre 47 y 48. La Plata, Argentina.

CITE THIS ARTICLE AS:

L. Farabello, A. Scarabino and F. Bacchi. "Numerical analysis of ice accretion on an airfoil: A case study", *Revista Facultad de Ingeniería Universidad de Antioquia*, no. 116, pp. 100-109, Jul-Sep 2025. [Online]. Available: https://www.doi.org/10.17533/udea.redin.20241145

ARTICLE INFO:

Received: April 25, 2024
Accepted: November 27, 2024
Available online: November 28, 2024

KEYWORDS:

Aircraft icing; computational fluid dynamics; airworthiness; aerodynamics

Hielo en aeronaves; dinámica de fluidos computacional; seguridad aérea; aerodinámica

ABSTRACT: The accumulation of ice on aircraft surfaces is known to endanger flight safety, which has driven the study and development of various methods to prevent this issue. A frequent problem aircrafts suffer is the ice accumulation on wings when flying across clouds with supercooled droplets. The shape and size of the ice accretion depend essentially on the flying speed, air temperature, number and size of microdroplets present in the atmosphere, and the exposure time to ice formation conditions. The numerical analysis of ice accretion involves differential equations for the resolution of the air velocity field, the transport of droplets, and their icing and melting. In this work, numerical models implemented in ANSYS CFD and Fensap-Ice codes are validated against experimental results and then applied to compute the ice formation on an MS(1)-0313 airfoil, used in a SAAB 340 wings, an aircraft that suffered a lethal accident in the Argentine Patagonia on May 18^{th}, 2011. The simulation parameters were chosen based on meteorological reports of that day and the type of clouds that were present at the time of the accident. The goal of this work is to apply Fensap-Ice to verify whether icing on the wings could have been the cause of the accident. The results of this study confirm that the hypothesis is highly probable.

RESUMEN: La acumulación de hielo sobre las superficies del avión es un fenómeno que atenta contra la seguridad en vuelo, lo que ha motivado el estudio y desarrollo de distintos medios para prevenirla. Un problema frecuente que sufren las aeronaves es la acumulación de hielo en las alas al volar a través de nubes con microgotas superenfriadas. La forma y tamaño de las formaciones de hielo dependen esencialmente de la velocidad de vuelo, la temperatura del aire, la cantidad y tamaño de las microgotas presentes en la atmósfera y el tiempo de exposición a las condiciones de formación de hielo. En este trabajo, los modelos numéricos implementados en los softwares comerciales ANSYS CFD y Fensap Ice fueron validados contra resultados experimentales y luego aplicados al cómputo de formación de hielo en el perfil aerodinámico MS(1)-0313, utilizado en las alas del avión SAAB 340. Uno de estos aviones sufrió un accidente fatal en la Patagonia, Argentina el 18 de mayo de 2011. Los parámetros para la simulación se definieron con base en los reportes meteorológicos de ese día y el tipo de nubes presentes en el sitio y a la hora del accidente. El objetivo de este trabajo es aplicar el código Fensap-Ice para verificar la posibilidad de que la formación de hielo en las alas haya sido la causa del accidente. Los resultados del estudio confirman esta hipótesis como muy probable.

1. Introduction

Flight safety of aircraft operating under natural icing conditions is a critical concern for aircraft manufacturers [1]. Aircraft can accrete ice on their aerodynamic surfaces when flying through clouds of supercooled water droplets. Liquid water may be cooled well below freezing point in the absence of a freezing nucleus. In this way, clouds may contain liquid water in the form of supercooled droplets for prolonged periods. Supercooled droplets will tend to freeze when they encounter ice particles or solid structures such as

* Corresponding author: Ana Scarabino
E-mail: scarabino@ing.unlp.edu.ar
ISSN 0120-6230
e-ISSN 2422-2844

DOI: 10.17533/udea.redin.20241145

aircraft. This process is responsible for the rapid growth of ice formations which cause aerodynamic and control problems for aircraft. The size and shape of the ice accretion on unprotected aerodynamic surfaces depend primarily on airspeed, temperature, water droplet size, liquid water content, and the time the aircraft has been operating in the icing condition [2]. Ice accretion on wings increases weight and aerodynamic drag, and decreases lift, reducing the overall aerodynamic performance. The adverse effects of ice accretion are not restricted to wings: AGARD´s 344 Report [3] covers the effects of ice accretion on wings, tail surfaces, engine inlets, and rotary wings.

Commercial flights can occasionally avoid clouds with supercooled droplets on their routes, but not at landing or take off. Aircrafts with a ceiling height under 10000 m cannot fly above these clouds. To deal with this situation, anti-icing systems were developed, based on two different concepts [3]: On medium-sized and large jet aircrafts, heating is typically applied in the leading edge by using bleed air from the engine compressors, either to evaporate all impinging water droplets (anti-icing) or to melt accreted ice at the surface (de-icing). Electrical heating and the injection of a freezing point depressant fluid are also options for different aircrafts.

For turboprop aircraft, the most usual de-icing devices are pneumatic boots. These are inflated cyclically to fracture and expel the ice accretion from the surface. A disadvantage of this method is that, for effective ice removal, the ice shapes must have a minimum thickness of about one centimeter, and this thickness and the aerodynamic deterioration that it causes must be tolerable for flight safety. A limitation is that, if the de-icing system is not activated within the operating range of ice thickness, it will not be able to remove the ice formation. Novel methods are being investigated, such as the use of ice-phobic or superhydrophobic coatings, as it is described in detail in [4].

The ice accretion process develops in different types of ice growing under diverse environmental conditions [3]. "Rime ice" results when supercooled water droplets freeze instantaneously on impact with any very cold wing surface This process creates a relatively low density porous ice with a distinctive opaque white appearance. The rime ice accretion process is relatively simple because the impacting droplets freeze and remain where they strike the surface. Rime ice usually forms at temperatures well below 0 ºC with small supercooled droplets. It tends to accumulate at the wing leading edge.

"Glaze ice" appears in conditions of high relative humidity, large supercooled droplets, and temperatures near 0 ºC. Glaze ice is transparent or translucent and typically has one or two horns. This characteristic appears because the liquid water that impinges the wing does not freeze instantaneously and slips downstream as it freezes.
Commonly, droplets in clouds appear in a range of sizes, so that a combination of both types of ice appears, in what is named "mixed ice". In this case, a portion of the droplets of smaller size freezes immediately forming rime ice, while the rest slips above freezing progressively as glaze ice. The final formation is also a combination of both types, with smaller horns than pure glaze ice and larger accumulations at the leading edge [5]. Figure 1 shows examples of the three types of ice accretion on wings.

The accumulation of ice on aircraft surfaces is a meteorological phenomenon that poses a significant threat to flight safety. Four primary factors that affect flight safety are mentioned in [4]: Degradation of aerodynamic performance, such as reduced maximum lift coefficient and lift curve slope, increased drag, and higher critical stall speed [6]; pitch instability, which lowers the airfoil's stall angle of attack and complicates flight [7]; unexpected maneuvers, such as rolling and overturning, caused by additional rolling moments from ice ridge formation beyond the ice protection device; and reduced control performance, such as increased stick force due to tailplane ice, which can impair maneuverability [7, 8].

Issues related to ice accretion and shedding in rotorcraft are addressed in [9], presenting a methodology to create a probability map of ice shedding trajectories on the engine intake and tail rotor planes, where an impact poses a significant risk to the vehicle operational safety.

The negative impact of ice accretion on an airfoil's aerodynamic performance can be reduced through proper airfoil design. It has been shown in [10] that a rise in the camber line and aft loading can increase the lift coefficient of an iced airfoil by up to 18%. In [11] it was reported that careful shaping of the slat and flap of a multi-element airfoil led to a 10% increase in the lift coefficient (CL).

Every year accidents are reported, both in civil and military aviation, private and commercial, where ice accretion is suspected to play a fundamental role. In August 2024, at the time this paper was being written, a twin-engine turboprop ATR 72 crashed in São Paulo, Brazil, resulting in the deaths of 57 passengers and the five crew members. Although it is too early to determine the cause of the accident, it has been confirmed that the weather conditions in the flight area favored ice accretion, leading to speculation that a failure in the de-icing system may have contributed to the tragedy [12]. Two of the worst commercial aviation accidents in Argentina (Austral Flight 2553, October 10th, 1997, and Sol Flight 5428, May 18^{th}, 2011) are believed to have been caused by ice formations.

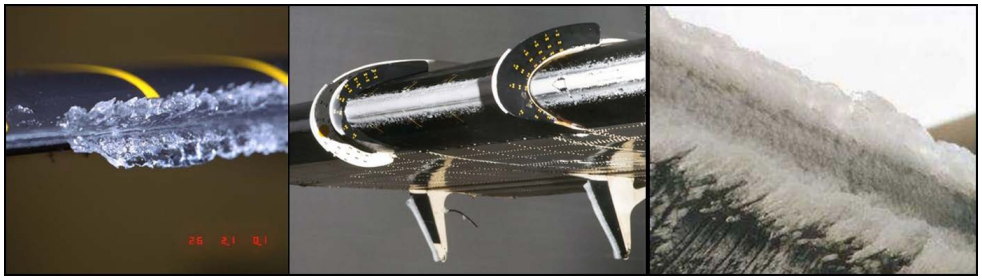

Figure 1 From left to right: glaze, rime, and mixed ice

Because of the human casualties and economic losses that these events cause, this problem is widely investigated by aircraft manufacturers, certification authorities, and different institutes and organisms.

The problem has been addressed by NASA, through tests in wind tunnels specially adapted to simulate the conditions of ice formation on wings [13]. Additionally, different codes have implemented numerical models for ice accretion, one of them being ANSYS Fensap-Ice [14], the one used for the results presented in this work. This code has been widely employed and validated for simulating ice accretion [15–17]. A growing number of articles present results of numerical simulations of the ice accretion on airfoils, wings, and other aircraft components, such as nacelles or propellers. In [18], a numerical method is developed for simulation of ice accretion based on potential flow and boundary layer computations for the air flow; in [19], experimental and numerical results for a NACA 0012 airfoil were compared, the latter obtained by analytical methods. Also, commercial and open-source CFD codes have implemented ice accretion models, which have been used in works such as [20, 21], and, more recently in [22]. In [23], results of different RANS and URANS models for a NACA 23012 airfoil with two ice shapes are presented, validated through comparison with the more advanced Zonal Detached Eddy Simulation method (ZDES), using ONERA´s elsA software. The study concluded that the Spalart-Allmaras turbulence model (the one used in this work) was the only RANS model among those assessed in the study, which converged efficiently towards steady-state whatever the flow condition considered. Spalart-Allmaras was also preferred over other available RANS models for its simplicity, as it introduces only one additional transport equation, and it captures the flow dynamics within the boundary layer, including the viscous sublayer where ice accretion begins [24].

We present in this paper the mathematical model employed for the numerical simulation of ice accretion on airfoils implemented in ANSYS Fensap-Ice, a comparison of our numerical results with the experimental ones of [13] at NASA´s Icing Research Tunnel, and, finally, the numerical results of ice accretion on the MS(1)-0313 airfoil, used by the SAAB 340 airplane at Sol Flight 5428, which crashed in an isolated Patagonian region in the province of Río Negro, Argentina, on May 18^{th}, 2011. The purpose of this work is to apply Fensap-Ice in order to evaluate the possibility that icing on the wings could have been the cause of the accident. The numerical model is first applied to simulate experiments carried out at NASA´s Glenn Research Center IRT wind tunnel, in order to calibrate the model by comparison of numerical and experimental results, and then applied to the MS(1)-0313 airfoil, under meteorological conditions similar to those reported at the crash site. Due to computational limitations, the study will be performed for a 5cm wing slice, with the wing mean chord, at cruising speed and altitude. Further details of this work are presented in [25].

2. Methodology

2.1 Mathematical model

Ice accretion poses a multiphase fluid problem involving two substances, air and water, with the latter present in two phases, liquid and solid. To solve this problem, temperature variations within the domain, especially at the solid walls, must be considered, as well as the interaction of the two fluid phases and the water icing and melting processes. The initiation of ice accretion is a random process mainly affected by atmospheric conditions, such as temperature, pressure, number, and size of droplets in clouds, as well as the aircraft's speed and surface temperature.

The computations performed with Fensap-Ice involve four stages following a sequence, as described in [26]. The differential equations to be solved at each stage are presented below.

- 1) Equations of conservation of mass, momentum, and energy are solved for the air motion. A "one-way interaction" is postulated, in which the droplets carried by air do not influence nor modify the air velocity field. Subindex a applies for air, so the mass (Equation 1), momentum (Equation 2), and energy

(Equation 3) conservation equations for this stage are:

$$\frac{\partial \rho_a}{\partial t} + \vec{\nabla} \cdot \left(\rho_a \vec{V_a} \right) = 0 \tag{1}$$

$$\left(\frac{\partial \rho_a u_{a,i}}{\partial t} + \frac{\partial \rho_a u_{a,i} u_{a,j}}{\partial x_j} \right) = \rho_a g_i - \frac{\partial P}{\partial x_i} + \mu_a \nabla^2 u_{a,i} + \frac{1}{3} \mu_a \frac{\partial}{\partial x_i} \vec{\nabla} \cdot \overrightarrow{V_a} \tag{2}$$

$$\frac{\partial}{\partial t} \left(\rho_a E_a \right) + \vec{\nabla} \cdot \left(\rho_a \vec{V_a} H_a \right) = \vec{\nabla} \cdot \left(k_a \left(\vec{\nabla} T_a \right) + V_{ai} \tau^{ij} \right) + \rho_a \vec{g} \cdot \vec{V_a} \tag{3}$$

$\vec{V_a}$ is the air velocity (with cartesian components $u_{a,i}$), ρ_a, the air density, μ_a, the air viscosity, E_a, the air internal energy, H_a, the air enthalpy, k_a, the air thermal conductivity, T_a, the air temperature, τ^{ij}, the air deviatoric stress tensor and. $\vec{g}$, the gravity acceleration.

To close the system, thermodynamic equations of state for the air, considered as a perfect gas, are included. The Spalart-Allmaras turbulence model, chosen for this study, includes one additional differential equation for the transport of turbulent viscosity [25].

- 2) From the inputs "Liquid Water Content" (LWC, mass of liquid water per unit volume of air) and "Median Volumetric Diameter" (MVD), a random distribution of droplets is generated on the previously computed airfield. Equations must be solved for the water droplets concentration (α) and velocity. The second subindex, ∞, stands for non-perturbed conditions far upstream from the airfoil. Equation (4) stands for water fraction mass conservation, and Equation (5) stands for water fraction momentum conservation.

$$\frac{\partial \alpha}{\partial t} + \vec{\nabla} \cdot \left(\alpha \vec{V_d} \right) = 0 \tag{4}$$

$$\frac{\partial \left(\alpha \vec{V_d} \right)}{\partial t} + \vec{\nabla} \cdot \left[\alpha \vec{V_d} \vec{V_d} \right] = \frac{C_D Re_d}{24K} \alpha \left(\vec{V_a} - \vec{V_d} \right) + \alpha \left(1 - \frac{\rho_a}{\rho_d} \right) \frac{1}{Fr^2} \vec{g} \tag{5}$$

Parameter (α) in Equations (4) and (5) represents the mean concentration of droplets in the flow, and Vd,a are respectively the temporal mean velocities of droplets (d) and air (a), the latter already computed at the previous stage. The first term at the right side of the equation represents the aerodynamic drag on the droplets of mean diameter d, which is proportional to the droplet's relative velocity in the air, its drag coefficient CD, its Reynolds number Red, and an inertial parameter K, which considers the deviation from Stokes´ law at moderate Reynolds numbers, defined in Equation (6) and Equation (7) as follows:

$$Re_d = \frac{\rho_d V_{a,\infty} \left\| \vec{V_a} - \vec{V_d} \right\|}{\mu_a} \tag{6}$$

$$K = \frac{\rho_d d^2 V_{a,\infty}}{18 L_\infty \mu_a} \tag{7}$$

In these definitions, ρ_d is the water density in droplets, μ_a, the air dynamic viscosity and d, the droplet diameter. The second term represents the gravity and buoyancy forces, which depend on the local Froude number, defined in Equation (8):

$$Fr = \frac{\| V_{a,\infty} \|}{\sqrt{L_\infty g}} \tag{8}$$

L_∞ is a characteristic length, equal to the airfoil chord for this analysis.

- 3) With the previously obtained droplets distribution and velocities, their impact and freezing on the airfoil are computed. At this stage, the equations to be solved are those of conservation of mass and energy, considering icing, melting, and evaporation, but only for the water on the airfoil surface. The conservation of mass is expressed in Equation (9) as follows:

$$\rho_f \left[\frac{\partial h_f}{\partial t} + \vec{\nabla} \cdot \left(\vec{V_f} h_f \right) \right] = V_\infty LWC\beta - \dot{m}_{evap} - \dot{m}_{ice} \tag{9}$$

$\vec{V_f}$ is the velocity of water at the top of the liquid layer on the airfoil, and h_f is the height or thickness of this liquid water layer. The three terms on the right side correspond respectively to the mass transfer for the droplets impingement (playing the role of a source term for the water layer) and liquid mass losses by evaporation and icing (sink terms for the water layer). Parameter β, called "droplet collection efficiency" is defined in Equation (10) as follows:

$$\beta = -\frac{\alpha \overrightarrow{V_d} \cdot \vec{n}}{(LCW)_\infty V_\infty} \tag{10}$$

Equation (11) stands for the conservation of energy:

$$\rho_f \left[\frac{\partial h_f c_f \tilde{T_f}}{\partial t} + \vec{\nabla} \cdot \left(\vec{V_f} h_f c_f \tilde{T_f} \right) \right] = \left[c_f \left(\tilde{T_\infty} - \tilde{T_f} \right) + \frac{\left\| \vec{V_d} \right\|^2}{2} \right] V_\infty LWC\beta - L_{\text{evap}} \dot{m}_{\text{evap}} - \left(L_{fusion} - c_s \tilde{T} \right) \dot{m}_{\text{ice}} + \sigma\varepsilon \left(T_\infty^4 - T_f^4 \right) - c_h \left(\tilde{T_f} - \tilde{T}_{\text{ice,rec}} \right) + Q_{\text{anti-icing}} \tag{11}$$

$\tilde{T_f}$ is the water temperature averaged in the liquid layer height; c_f, the specific heat of liquid water;

$\tilde{T}_\infty$, the temperature of droplets far upstream from the airfoil; $L_{\text{evap,fusion}}$, are respectively the latent heat of evaporation and fusion; C_S is the specific heat of ice (solid phase); σ„ Boltzmann constant $\left(=5.67\text{e}-8\ \text{W/m}^2\ \text{K}^4\right)$; ε, the solid emissivity; c_h, the convective heat transfer coefficient; $\tilde{T}_{ice,rec}$, the ice temperature corrected by a recovery factor, which considers the effect of energy losses due to friction, and $Q_{\text{anti-icing}}$, the anti-icing heat flux.

The first three terms on the right side of the equation model the heat transfer generated by droplets impingement, evaporation, and icing. The last three terms quantify heat transfer by radiation, convection, and conduction when anti-icing heating systems are acting. The variables to be solved are the water layer thickness (h_f), the water equilibrium temperature $\left(\widetilde{T}_f\right)$, and the mass of accumulated ice (m_{ice}). $\tilde{T}_{\text{ice, rec}}$ is the temperature corrected by a recovery factor which considers the effect of energy losses due to friction. The liquid layer and its mass exchanges are illustrated in Figure 2.

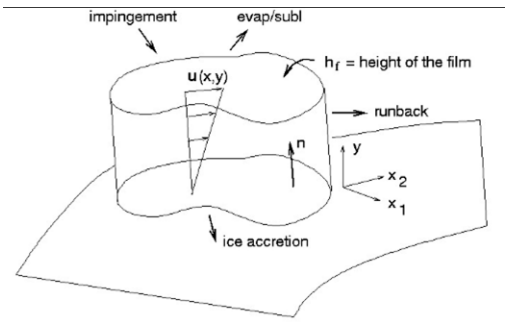

Figure 2 Scheme of the mass transfer processes at the freezing water layer on the airfoil Source: [26]

- 4) After an interval to be determined, the solid geometry is updated considering the ice layer thickness on the airfoil surface, the domain is re-meshed, and the sequence starts over with the modified geometry and boundary conditions on the airfoil.

2.2 Numerical model and validation

To validate the numerical model, simulations were carried out reproducing the experiments of [13] in NASA´s Glenn Research Center IRT wind tunnel, for an NLF-0414 airfoil. In order to reproduce an approximately bidimensional flow, a non-structured mesh of approximately 3e5 elements was generated, in a domain of 0.05m of lateral depth with lateral boundary conditions of symmetry. To capture the ice layer evolution, the airfoil boundary layer must be finely discretized. In this problem, precision and good matching of numerical and experimental results were obtained with a first element height of 1e-6 m and a growing factor of 1.1 for the adjacent elements. This discretization also matched the requirements of the Spalart-Allmaras turbulence model (first element y+ ⩽ 1). Figure 3 shows the domain and boundary conditions, and Figure 4 shows details of the mesh. Table 1 and Table 2 summarize the simulation parameters, following the guidelines of [27].

A mesh independence analysis was performed for the clean NLF-0414 airfoil in dry air at the temperature and velocity used in the NASA 622 experiment $(\text{T}=-5°\text{C}$ and $\text{V}=66.9\ \text{m/s})$. Meshes with element counts ranging from approximately 47000 to 350000 were employed, resulting in variations in lift and drag coefficients of less than 1%, as shown in Table 3. However, the fine discretization required for an accurate simulation of ice accretion (1×10^{-6} m for the first element height and a growing factor of 1.1 for the adjacent elements) led to the decision to use the finest mesh.

This mesh was also used to test the optimal time steps and intervals between successive mesh updates needed because of ice accumulation. After testing different remeshing intervals, it was concluded that an interval of 120s of physical time between successive remeshing was adequate. Figure 5 shows the ice accumulation after 360 seconds by updating the mesh once at 354s, every 120s, and every 60s, for the NLF-0414 airfoil under conditions of rime ice formation.

For the simulations of airfoil MS(1)-0313 in flight conditions, a similar mesh was generated, in a domain with a streamwise extension of 25 chord lengths and 20 chord lengths of height. The angle of attack and air speed for the simulation were those of cruise operating conditions, whereas the flying height of 1500m was defined after the accident Report of the Argentina National Air Accident Investigation Authorities [28]. The temperature was reported by the Neuquén Airport meteorological station, the closest one to the accident location, which also shares the topographical characteristics of the site. The liquid water content in droplets (LWC) and their median volumetric diameter (MVD) were obtained from Ap. C of FAR 25 Regulation [29], for the flight altitude and type of stratiform clouds present on the day of the accident. ANSYS Fensap-Ice uses the 10-bin Freezing Drizzle Drop Size Distributions defined in FAR AC 25-28 [30].

Table 4 shows the air speed, stagnation and static temperature, angle of attack, chord, time of exposure to icing conditions (t_exp.), MVD, and LWC of the performed simulations. The boundary conditions for the simulations of NASA´s experiments are those reported for the wind

Table 1 Technical characteristics of the sensors used to monitor the operation of the chiller

Parameter	Value
Continuous Fluid Phase	Air - incompressible (T and rho depending on case)
Droplets	Water-liquid (T depending on cas)
Solid Phase	Iced water
Pressure-Velocity Coupling	Coupled
Gradient	Least Squares Cell-Based
Pressure	Second Order
Momentum	Second Order Upwind
Transitional formulation	Second Order Implicit
Solver	Pressure Based
Velocity formulation	Absolute
Time	Transient
Turbulence model	Spalart-Allmaras

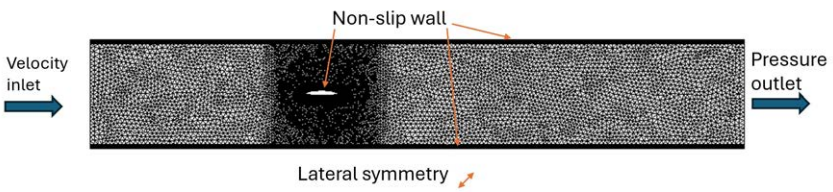

Figure 3 Domain, mesh, and boundary conditions for the numerical simulations of the wind tunnel experiments

Table 2 Boundary conditions

Tunnel and airfoil	Non-slip wall
Inlet	Velocity inlet, V depending on case
Outlet	Pressure outlet. P = 0 (rel.)

Table 3 Mesh independence analysis

Mesh elements	**0.47 10^5**	**1 10^5**	**2.1 10^5**	**3.5 10^5**
C_L	0.4634	0.4661	0.4659	0.4677
C_D	0.0105	0.0105	0.0105	0.0104

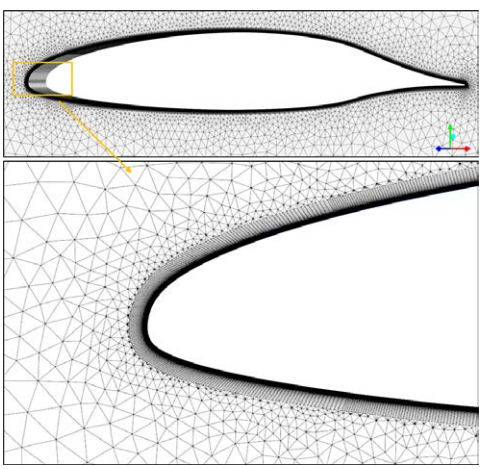

Figure 4 Mesh details: Side perspective view (above) and lateral view of the leading edge (below)

tunnel tests in [13]. Magnitudes such as LWC, MVD, and time of exposure (t_exp) are expressed in the usual units found in the literature.

3. Results

Several cases were run under both rime and glaze ice conditions. Once the model was optimized and the numerical results matched NASA's experimental ones, the simulations for airfoil MS(1)-0313 were carried out, with the air velocity, temperature, MVD and LWC shown in Table 1, estimated for a flying height of 14000ft (4267m) in the Río Negro region where the accident occurred on May 18^{th}, 2011. Figure 6 shows the ice accretion obtained at NASA´s experiments and our numerical simulations under conditions of glaze ice (test 622) and rime ice (test 627). The different contour lines shown in the experimental results correspond to ice accumulation at 120, 240, and 360s (2, 4, and 6 min.), respectively.

Although the ice shapes presented slight differences, mainly in the extension of ice accretion, which was underestimated in the numerical results, the maximum ice thickness and its location showed good agreement between the experimental and the numerical results.

Table 5 presents and compares both the experimental and numerical values of lift and drag coefficients for the airfoils studied, including the variation observed under iced condition. Despite minor differences related to ice

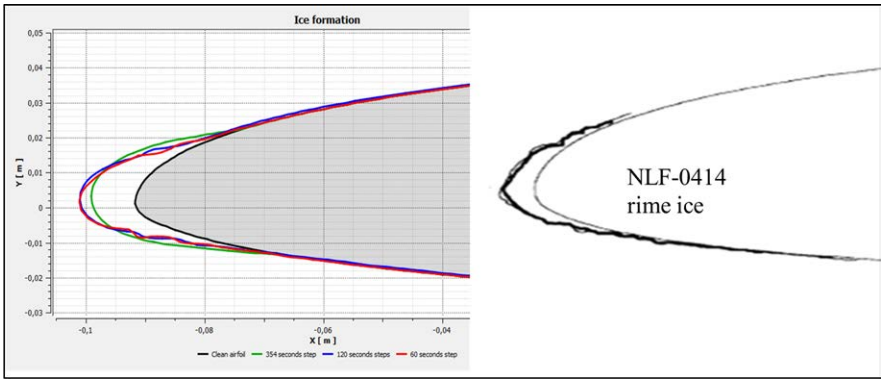

Figure 5 Comparison of final results after 360s (6 minutes) of exposure to rime ice conditions with remeshing at 354s (green), 120s (blue) and 60s (red). The experimental shapes on the right correspond to three different tests [13]

Table 4 Simulation parameters

Case	To (°C)	T (°C)	V (m/s)	α (o)	c (m)	t_exp (min.)	MVD (μm)	LWC (g/m^3)
NASA 622 (glaze)	-2.8	-5	66.9	0.3	0.9144	6	20	0.54
NASA 627 (rime)	-7.8	-10	66.9	0.3	0.9144	6	20	0.44
MS(1)-0313	-4.6	-13	130	0	1.95	8	32.5	0.56

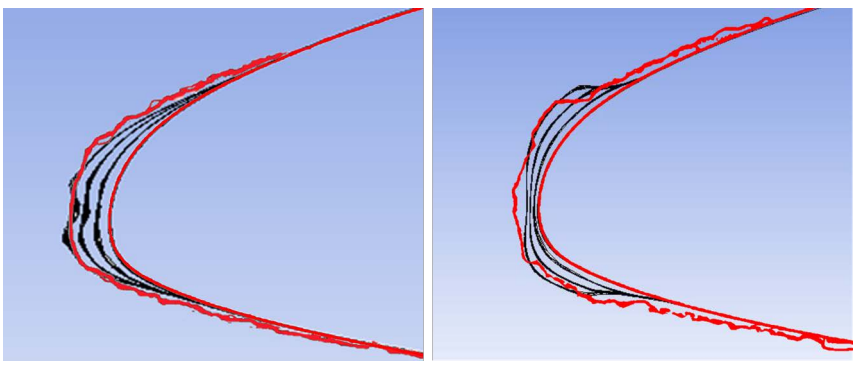

Figure 6 Numerical (contours every 2 minutes) -in black- and experimental -in red- results, for conditions of rime (left) and glaze (right) ice for an NLF-0414 airfoil

accumulation on the airfoil, the agreement between the numerical results of this study and the experimental values reported in [13] was very good.

Figure 7 shows the computed ice growth on airfoil MS(1)-0313. The different contour lines show its evolution in intervals of 120s (2 minutes). The final shape is obtained after 480s (8 minutes) of flight under these conditions. The central image is a 3D view of the airfoil leading edge, and the plot on the right the final ice thickness distribution as a function of coordinate y.

The ice distribution, with two "horns", suggests a prevalence of glaze ice. The maximum height is 0.025m (25mm) and its mean growth rate is $5 * 10^{-5}$ m/s (3 mm/min). The upper and lower "horns" change the airfoil aerodynamic characteristics, causing local boundary layer detachments with recirculation bubbles, as seen in Figure 8, which alter the pressure distribution (Figure 9), increasing the frontal stagnation area and generating suction right behind the ice horns. This flow pattern increases aerodynamic drag and reduces lift. Table 5 reports the lift and drag coefficients measured at NASA's experiments and those computed for the MS(1)-0313, clean and with ice accumulation, and quantifies the difference between experimental and numerical results as well as the degradation of both coefficients. We see that the percentages of drag increase and lift reduction of MS(1)-0313 airfoil are comparable to those of NLF-0414 airfoil as measured in experiments.

4. Discussion and conclusions

With the mathematical and numerical tools implemented in the Fensap-Ice module of ANSYS CFD, the possibility

Table 5 Changes in lift and drag coefficients due to ice accretion

Airfoil		Clean (Exp.)	Clean (CFD)	% Dif.	Iced (Exp.)	Iced (CFD)	% Dif.	Variation iced (CFD)	% Variation Iced (CFD)
NLF-0414 (rime)	CL	0.478	0.4797	0.356	0.443	0.4277	3.454	-0.052	-10.84
	CD	0.0105	0.0105	0.000	0.0167	0.0169	1.198	0.0064	61.27
NLF-0414 (glaze)	CL	0.479	0.4677	2.359	0.44	0.4277	2.795	-0.04	-8.55
	CD	0.0105	0.0105	0.000	0.0204	0.0203	0.490	0.0098	93.65
MS(1)-0313	CL	—	0.353		—	0.324		-0.029	-8.22
	CD	—	0.009		—	0.0148		0.005	64.44

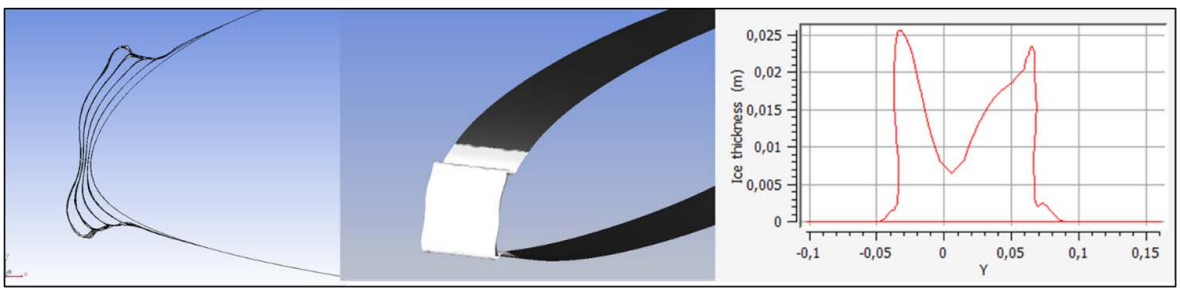

Figure 7 Ice accumulation on the leading edge of airfoil MS(1)-0313. On the right, ice thickness distribution

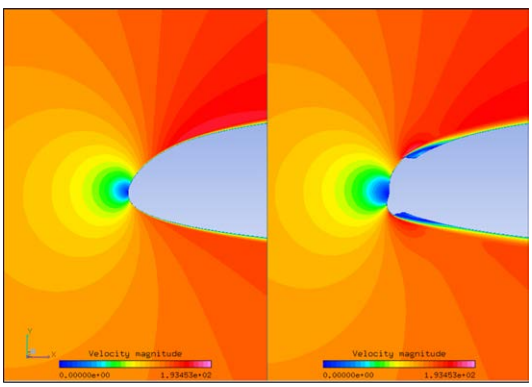

Figure 8 Detail of the velocity field around the leading edge for the MS(1)-0313 airfoil clean (left) and after 8 min. of ice accumulation (right)

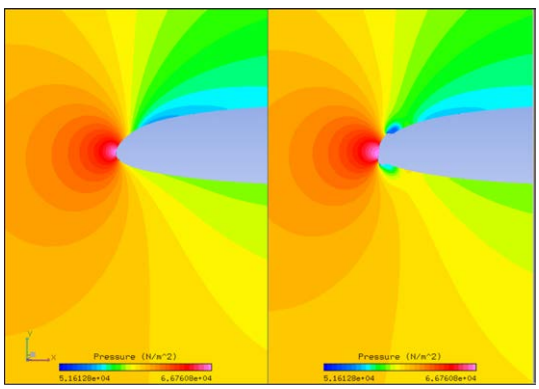

Figure 9 Detail of the pressure field around the leading edge for the MS(1)-0313 airfoil clean (left) and after 8 min. of ice accumulation (right)

of ice accretion on the SAAB MS(1)-0313 airfoil could be investigated. The numerical model was validated by comparisons with experimental results published by NASA. The computed changes in lift and drag coefficients due to ice accumulation on the MS(1)-0313 airfoil were comparable with those found for the NLF-0414 airfoil in wind tunnel experiments. Results showed that ice formation significantly impacts flight performance: airfoil drag increases by over 60%, requiring more thrust to maintain speed. The added weight from ice also raises the aircraft's overall weight, while the lift coefficient decreases by 8 to 10%.

The numerical results showed that, under the meteorological conditions implemented for the simulation of the MS(1)-0313 airfoil of SAAB 340 airplanes, the ice accumulation was rapid and intense, with a mean growth rate of 3 mm/min., which would stress the SAAB 340´s anti-icing boot system. The results of the simulation reinforce the suspicion that severe icing was one of the main causes of the accident of Sol flight 5428 on May 18^{th}, 2011.

The results also highlight the need to strengthen meteorological alerts for conditions of high probability of severe ice formation and to improve de-icing systems, such as pneumatic boots, to address rapid ice accumulation.
The work demonstrates that numerical simulation through CFD, among its many applications, can contribute to aviation accident investigation when ice formation is suspected to be a factor. It can also be used to enhance the performance of various anti-ice protection systems,

thereby contributing to aviation safety at a significantly lower cost compared to experimental testing, although it does not replace the necessary flight tests.

Future work includes applying the acquired knowledge and capabilities for studying the ice formation and accumulation on different aircraft components as well as other systems affected by ice, such as transmission lines and wind turbine blades, and the implementation of anti-ice or de-icing protection systems.

Declaration of competing interest

We declare that we have no significant competing interests including financial or non-financial, professional, or personal interests interfering with the full and objective presentation of the work described in this manuscript.

Funding

The author(s) received no financial support for the research, authorship, and/or publication of this article.

Author contributions

L. Farabello: Collected the meteorological data and configured and ran the ANSYS CFD and Fensap-Ice simulations, carrying out the pre- and postprocessing of results. A. Scarabino: Contributed to the theoretical work and analysis of results and wrote the paper. F. Bacchi: Provided the instruction in CFD techniques and Ansys Fluent and Fensap-Ice training and improved the quality and accuracy of the mesh and setup of the numerical model, and the postprocessing of results.

Data available statement

Some or all data, models, or code that support the findings of this study are available from the corresponding author upon reasonable request.

References

[1] Y. Cao, W. Tan, and Z. Wu, "Aircraft icing: An ongoing threat to aviation safety," *Aerospace Science and Technology*, vol. 75, 2018. [Online]. Available: https://doi.org/10.1016/j.ast.2017.12.028

[2] M. B. Bragg and E. Loth, "Effects of large-droplet ice accretion on airfoil and wing aerodynamics and control," Office of Aviation Research, Washington, D. C, Tech. Rep. DOT/FAA/AR-00/14, March 2000. [Online]. Available: https://apps.dtic.mil/sti/tr/pdf/ADA379331.pdf

[3] N. A. T. Organization, "Ice accretion simulation," Advisory Group for Aerospace Research & Development AGARD, Neuilly Sur Seine, France, Tech. Rep. AGARD-AR-344, 1997. [Online]. Available: https://www.sto.nato.int/publications/AGARD/Forms/AGARD

[4] S. Mousavi, F. Sotoudeh, B. Chun, B. J. Lee, N. Karimi, and S. A. Faroughi, "The potential for anti-icing wing and aircraft applications of mixed-wettability surfaces - a comprehensive review," *Cold Regions Science and Technology*, vol. 217, 2024. [Online]. Available: https://doi.org/10.1016/j.coldregions.2023.104042

[5] Z. Janjua, B. Turnbull, S. Hibberd, and K. Choi, "Mixed ice accretion on aircraft wings," *Physics of Fluids*, vol. 30, no. 2, 2018. [Online]. Available: https://doi.org/10.1063/1.5007301

[6] F. Piscitelli, S. Palazzo, and F. D. Nicola, "Icing wind tunnel test campaign on a nacelle lip-skin to assess the effect of a superhydrophobic coating on ice accretion," *Applied Sciences*, vol. 13, no. 8, 2023. [Online]. Available: https://doi.org/10.3390/app13085183

[7] D. I. Ignatyev, A. N. Khrabrov, A. I. Kortukova, D. A. Alieva, M. E. Sidoryuk, and S. G. Bazhenov, "Interplay of unsteady aerodynamics and flight dynamics of transport aircraft in icing conditions," *Aerospace Science and Technology*, vol. 104, 2020. [Online]. Available: https://doi.org/10.1016/j.ast.2020.105914

[8] M. Muhammed and M. S. Virk, "Ice accretion on rotary-wing unmanned aerial vehicles - a review study," *Aerospace*, vol. 10, no. 3, 2023. [Online]. Available: https://doi.org/10.3390/aerospace10030261

[9] B. Sengupta, R. L. Prince, M. Y. Cho, C. Son, T. Yoon, K. Yee, and R. S. Myong, "Computational simulation of ice accretion and shedding trajectory of a rotorcraft in forward flight with strong rotor wakes," *Aerospace Science and Technology*, vol. 119, 2021. [Online]. Available: https://doi.org/10.1016/j.ast.2021.107140

[10] H. Li, Y. Zhang, and H. Chen, "Optimization design of airfoils under atmospheric icing conditions for uav," *Chinese Journal of Aeronautics*, vol. 35, no. 4, 2022. [Online]. Available: https://doi.org/10.1016/j.cja.2021.04.031

[11] J. Dai, H. Li, Y. Zhang, and H. Chen, "Optimization of multi-element airfoil settings considering ice accretion effect," *Chinese Journal of Aeronautics*, vol. 36, no. 2, 2023. [Online]. Available: https://doi.org/10.1016/j.cja.2022.07.016

[12] Wikipedia, "Voepass linhas aéreas flight 2283," n.d., retrieved August 21, 2024. [Online]. Available: https://en.wikipedia.org/wiki/Voepass_Linhas_A%C3%A9reas_Flight_2283

[13] H. Addy, "Ice accretions and icing effects for modern airfoils," NASA, Tech. Rep., 2000, nASA Technical Report 2000-210031.

[14] W. Habashi, F. Morency, and H. Beaugendre, "Fensap-ice: A second generation 3d cfd based in-flight icing simulation system," SAE Technical Paper Series, Tech. Rep., 2003. [Online]. Available: https://doi.org/10.4271/2003-01-2157

[15] K. Nakakita, S. Nadarajah, and W. Habashi, "Toward real-time aero-icing simulation of complete aircraft via fensap-ice," *Journal of Aircraft*, vol. 47, no. 1, 2010. [Online]. Available: https://doi.org/10.2514/1.44077

[16] H. Beaugendre, F. Morency, and W. G. Habashi, "Fensap-ice's three-dimensional inflight ice accretion module: Ice3d," *Journal of Aircraft*, vol. 40, 2022. [Online]. Available: https://doi.org/10.2514/2.3113

[17] W. Yoon, J. Kim, C. Chung, and J. Park, "Numerical study on prediction of icing phenomena in intake system of diesel engine: Operating conditions with low-to-middle velocity of inlet air," *Energy*, vol. 248, 2022. [Online]. Available: https://doi.org/10.1016/j.energy.2022.123569

[18] M. Alexandrescu and N. Alexandrescu, "Numerical simulation of ice accretion on airfoil," *INCAS - Bulletin*, vol. 1, 2009. [Online]. Available: https://doi.org/10.13111/2066-8201.2009.1.1.4

[19] F. Meng, Z. C. W. D., and M. H., "Experimental and numerical investigation of ice accretion on airfoil," in *Fourth International Symposium on Physics of Fluids (ISPF4)*, vol. 19, 2012. [Online]. Available: https://doi.org/10.1142/S2010194512008793

[20] Y. Cao, C. Ma, Q. Zhang, and J. Sheridan, "Numerical simulation of ice accretions on an aircraft wing," *Aerospace Science and*

Technology, vol. 23, 2012. [Online]. Available: https://doi.org/10.1016/j.ast.2011.08.004

[21] S. Li, J. Qin, M. He, and R. Paoli, "Fast evaluation of aircraft icing severity using machine learning based on xgboost," *Aerospace*, vol. 7, no. 36, 2020. [Online]. Available: https://doi.org/10.3390/aerospace7040036

[22] S. Strijhak, D. Ryazanov, K. Koshelev, and A. Ivanov, "Neural network prediction for ice shapes on airfoils using icefoam simulations," *Aerospace*, vol. 9, no. 96, 2022. [Online]. Available: https://doi.org/10.3390/aerospace9020096

[23] M. Costes and F. Moens, "Advanced numerical prediction of iced airfoil aerodynamics," *Aerospace Science and Technology*, vol. 91, 2013. [Online]. Available: https://doi.org/10.1016/j.ast.2019.05.010

[24] P. Spalart and S. Allmaras, "A one-equation turbulence model for aerodynamic flows," *Recherche Aerospatiale*, vol. 1, 1994. [Online]. Available: https://doi.org/10.2514/6.1992-439

[25] L. A. Farabello, "Análisis computacional de formación de hielo en perfiles aerodinámicos," Universidad Nacional de La Plata, Tech. Rep., 2019. [Online]. Available: http://sedici.unlp.edu.ar/handle/10915/121536

[26] A. INC., *ANSYS Fensap-Ice User Manual V. 18.1*, 2017. [Online]. Available: https://ansyshelp.ansys.com/public/account/secured?returnurl=/Views/Secured/corp/v242/en/fensap_manual/fensap_manual.html

[27] J. D. Rosero-Ariza, J. L. Chacón-Velasco, and G. González-Silva, "Comparative cfd analysis of six vawt turbines in the chicamocha canyon," *Revista Facultad de Ingeniería, Universidad de Antioquia*, no. 113, 2024. [Online]. Available: https://www.doi.org/10.17533/udea.redin.20240413

[28] JIAAC, "Technical report 096/2011: "accident that occurred on 18 may 201, aircraft saab 340 a, lv-cej"," Aircraft Saab 340 A, Tech. Rep., Mar. 2015. [Online]. Available: https://asn.flightsafety.org/asndb/321116

[29] FAR/CS, "Aircraft icing: Appendix c to part 25," FAR/CS 25 Airworthiness Standards: Transport Category Airplanes, Tech. Rep., 2014. [Online]. Available: https://www.ecfr.gov/current/title-14/chapter-I/subchapter-C/part-25?toc=1

[30] FAR/AC, "Far/ac 25/28: Compliance of transport category airplanes with certification requirements for flight in icing conditions," Federal Aviation Administration, Tech. Rep., October 2014. [Online]. Available: https://www.faa.gov/regulations_policies/advisory_circulars/index.cfm/go/document.information/documentID/1019691